# MODELLING AND EVALUATION OF THE INFLUENCE OF END-STOPS IMPACTS ON RESPONSE SIGNAL IN A VIBRATION ISOLATING SYSTEM

Radúz Zahoranský, Juraj Stein*

*The end-stops in vibration isolation systems function as a structural constraint of the operational range. If engaged, the force response to the deformation exhibits a progressive growth. Mathematical approximation of end-stops characteristic is usually realized by a non-linear function of the exerted displacement. The engagement of end-stops changes system dynamic properties. Presence of general damping reduces the negative effect of end-stops. Several approaches to end-stops modelling and to approximate solution of resulting system equation are introduced, assuming certain region of linear restoring force. In real situation, the end-stops are not fully able to prevent hard impacts onto the solid operational constraints. The modelling of this phenomenon using the so-called penalty approach is described in the next section of the paper. Simulation analysis provides some insight into influence of linear viscous and non-linear friction damping. In the final part above described methods are compared while subjected to same excitation signal. In the conclusion some hints to practical application of results are indicated.*

Key words: *vibration isolation, non-linear system, end-stops, operational limits, viscous damping, dry-friction damping*

## 1. Introduction

A vibration-isolation system (VIS) of a modern suspended driver's seat contains components that restrict the range of possible motion to certain limits. The limiting components usually are rubber blocks with progressive force response on their deformation. Moreover, structural limits constrain the maximal available range of motion (stroke).

For modelling purposes, the influence of end-stops has to be analysed. Measurement, identification and analysis of such a structural element should be conditioned by the extent of its impact on overall system performance. If the relative displacement during standard excitation levels reaches into the end-stops region these must be included in the system model. Thorough analysis of their interaction with other system structural elements must be undertaken. The progressive increase of the spring force induces a functional dependence of the system resonance frequency on the amplitude of actual displacement as illustrated in [8]. Further on the influence of the hard structural limits should be assessed too. All this is subject of the following contribution.

* R. Zahoranský, J. Stein, Institute of Materials and Machine Mechanics of Slovak Academy of Sciences, Račianska 75, SK – 831 02 Bratislava, Slovak Republic

## 2. Identification of end-stops parameters

### 2.1. System description

The general structure of a horizontal VIS of a modern driver's seat usually consists of a linear spring with spring constant $k_{\mathrm{L}}$, viscous damper with assumed linear damping constant $b$, dry-friction component, described conventionally by the friction coefficient $\mu_{\mathrm{k}}$, and the end-stops – Figure 1. All these components are supposed to have symmetrical characteristics. The system is subjected to base excitation in the $x$-direction by displacement $u(t)$. The relative displacement $x_{\mathrm{r}}$ of such a system has essentially three regions (Figure 1):

i. a region $(-x_{\mathrm{L}}, +x_{\mathrm{L}})$ in which the attached spring can be assumed to be linear,
ii. $(-x_{\mathrm{op}}, -x_{\mathrm{L}})$ and $(+x_{\mathrm{L}}, +x_{\mathrm{op}})$ regions, in which the rubber end stops with progressive force/deflection characteristics come into action in addition to the spring influence,
iii. a region in excess of the operational range $(-x_{\mathrm{op}}, +x_{\mathrm{op}})$ where the operational limits are hardly hit.

Note the fact, that due to the construction of the frame itself both the end-stops and structural limits had to be assumed and modelled independently.

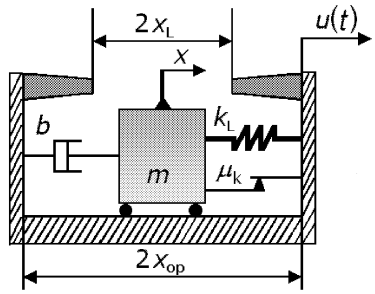


*Fig.1: Illustration of the horizontal VIS model with the end-stops (description see text)*

Quasi-static measurement of the response force over the exerted displacement up to operational limit is used in practice to conventionally describe the VIS properties. This measurement provides a characteristic hysteretic curve. Examples of experimentally measured hysteretic curves, supplied by a VIBSEAT project partner, are presented in Figure 2. Each of these two plots corresponds to a different arrangement of vibration-isolation mechanism without a hydraulic damper. Hence the extent of hysteresis represents energy dissipation, which can be considered to be predominantly due to the friction damping. The presence of similar system stiffness linear ranges $(-x_{\mathrm{L}}, +x_{\mathrm{L}})$ is clearly seen in both courses. Also the influence of end stops and their non-linear force-deflection characteristics is clearly seen. The static component of the friction force was identified from a span in the dwell point. The difference in the measured courses appears in the progressivity of the non-linear region as well as in the area that is proportional to the dissipated energy. Course 2 appertains to a suspension system, which is stiffer and has a less damped response, as the friction damping is significantly reduced in comparison to the system represented by the course 1.

### 2.2. Modelling of the end-stops characteristic

The main task of the identification of the end-stops is estimation of the unknown parameters of a selected regression model. The modelled mathematical approximation should

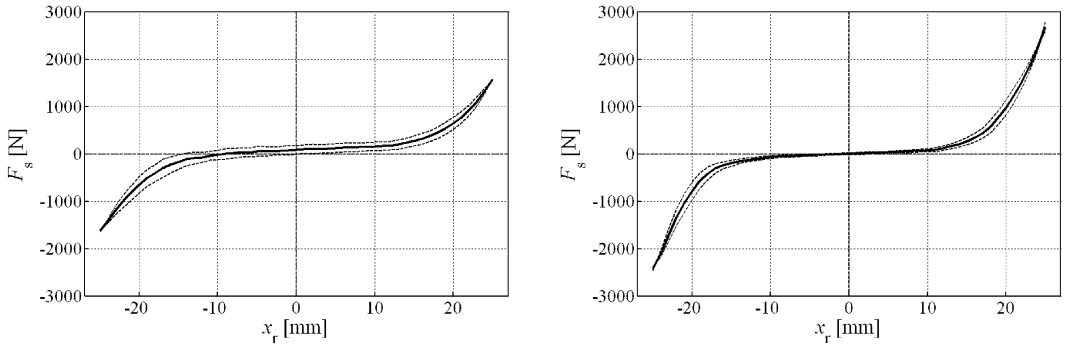


*Fig.2: Measured hysteretic curves for two different horizontal VIS of a driver's seat*

respect all the physical relations that can be assumed from measured data. On the other hand selected model should be easily applicable, i.e. it should be simple and physically transparent. Frequently used polynomial model should have a minimal number of terms. In [7] and [8] for a similar system quadratic function of the end-stop deformation is assumed to be an optimal mathematical model obtained by the least squares method (LSM). Due to tolerances estimated from the measurements of the static force proper and more detailed analysis of the optimal functional dependence became a topical task. Five independent models were assumed [9]:

- exponential model with unknown constant $A_1$ and exponent $\beta$ – Eq. (1);
- asymptotical exponential model with unknown constant $A_2$ and exponent $\beta$ – Eq. (3);
- a general $\alpha$-power model, unknowns: constant $A_3$ and power $\alpha$ – Eq. (4);
- quadratic model with a single unknown constant $k_{\mathrm{NLq}}$ and with power $\alpha = 2$ – Eq. (6);
- cubic model with a single unknown constant $k_{\mathrm{NLc}}$ and with power $\alpha = 3$ – Eq. (7).

Formula, defining $F_{\mathrm{s,NL}}$ as an exponential function of the end-stop displacement $\Delta$ is:

$$F_{\mathrm{s,NL}} = A_1 \, \lambda_1 \, \mathrm{e}^{\beta \Delta} \ , \tag{1}$$

where

$$\lambda_1 = \mathrm{sign}(x_\mathrm{r}) \quad \text{for} \quad |x_\mathrm{r}| \geq x_\mathrm{L} \ , \qquad \lambda_1 = 0 \quad \text{for} \quad |x_\mathrm{r}| < x_\mathrm{L} \ .$$

The variable $\Delta$ denotes the absolute deformation of the end-stops, i.e. displacement in the non-linear region ($|x_\mathrm{r}| > x_\mathrm{L}$), defined as $\Delta = |x_\mathrm{r}| - x_\mathrm{L}$. The dimension of the non-linear stiffness coefficient $A_1$ is [N].

For the purpose of the LSM application, the *absolute* value of Eq. (1) can be transformed into its logarithmic form:

$$\ln(F_{\mathrm{s,NL}}) = a_1 + \beta \, \Delta \ , \tag{2}$$

where $a_1 = \ln A_1$.

Asymptotical exponential law is expressed in similar way as Eq. (1):

$$F_{\mathrm{s,NL}} = A_2 \, \lambda_1 \, (\mathrm{e}^{\beta \Delta} - 1) \ , \tag{3}$$

while the dimension of the stiffness coefficient $A_2$ is again [N]. However, as the linearization by using logarithm is not possible, its application in the LSM identification procedure is rather difficult. For this reason it is not considered in the further analysis.

General formula of the non-linear restoring spring force $F_{\mathrm{s,NL}}$ in the $\alpha$-power form is:

$$F_{\mathrm{s,NL}} = A_3 \, \lambda_1 \, \Delta^{\alpha} \ , \tag{4}$$

while the unit of $A_3$ is $[\mathrm{Nm}^{-\alpha}]$.

Logarithm of the absolute value of Eq. (4) for $|x_{\mathrm{r}}| \geq x_{\mathrm{L}}$ leads to a linear course in the logarithmic scale [2]:

$$\ln(F_{\mathrm{s,NL}}) = a_3 + \alpha \, \ln \Delta \ , \tag{5}$$

where $a_3 = \ln A_3$.

As shown further, the choice of value $\alpha = 2$ turned out to be useful for following analysis, as the quadratic dependence of the restoring force fitted the experimental curve with sufficient precision. The non-linear end-stop spring force is then for $|x_{\mathrm{r}}| > x_{\mathrm{L}}$ expressed as:

$$F_{\mathrm{s,NL}} = k_{\mathrm{NLq}} \, \lambda_1 \, (|x_{\mathrm{r}}| - x_{\mathrm{L}})^2 \ , \tag{6}$$

while the unit of $k_{\mathrm{NLq}}$ is $[\mathrm{Nm}^{-2}]$.

Also the cubic expression ($\alpha = 3$) according to Eq. (4) was tested, for which the term $k_{\mathrm{NLc}}$ is:

$$F_{\mathrm{s,NL}} = k_{\mathrm{NLc}} \, \lambda_1 \, (|x_{\mathrm{r}}| - x_{\mathrm{L}})^2 \ , \tag{7}$$

while the unit of $k_{\mathrm{NLc}}$ is $[\mathrm{Nm}^{-3}]$.

Other approximations could be used, however, as shown further, the substitutions using the power laws of Eqs. (6), (7) furnished a sufficiently accurate non-linearity approximation, so there seemed no need to further explore other approximations.

### 2.3. Modelling of the operational limits by the penalty approach

As was seen in the experimental signals from laboratory measurements, supplied by VIBSEAT project partner, the relative displacement of motion of the described vibration-isolation system might even reach the operational limits of the system, so that $|x_{\mathrm{r}}| \geq x_{\mathrm{op}}$. The stiff operational limits represent a structural constraint for the oscillatory motion. The conclusion is such that for the certain conditions, i.e. either high level of excitation, excitation of resonant oscillations or a weak damping of the system, even the elastic end-stops are not sufficient in absorbing and converting all the kinetic energy of the moving mass. Consequently a hard hitting on the solid stops appears, resulting in extreme peaks in the response acceleration signal. Modelling of such a phenomenon is associated with incorporation of an additional high stiffness elastic element. In practice it can be strongly disadvantageous to extend the actual model by an additional degree of freedom, as the identification of parameters from available data would be too complicated or even impossible. A penalty function or barrier function are simple mathematical procedures used in the optimisation theory to describe this situation [6]. They can be easily adapted to be applied as a realization of the stiff operational limits in the so-called penalty approach. This method is broadly analysed in [3]. It is found to be reliable, simple, and beneficial for the purpose of mathematical modelling. The barrier force would be applied as the relative displacement $x_{\mathrm{r}}$ approaches the operational range $x_{\mathrm{op}}$ from within a given small interval $(x_{\mathrm{op}} - \varepsilon, x_{\mathrm{op}})$ [6]. The penalisation using the penalty force $P$ represents a virtual sharply rising restoring force component

in total restoring force $F_{\mathrm{s,PF}}$ (physical dimension [N]) – see left part of expression Eq. (8), which mathematically sanctions the exceeding of the allowed operational range $x_{\mathrm{op}}$.

For this concrete system a simple realization of the penalty force is an additional force term added to the original restoring force $F_{\mathrm{s}}$ for $|x_{\mathrm{r}}| > x_{\mathrm{op}}$ – the right part of the expression Eq. (8):

$$F_{\mathrm{s,PF}} = F_{\mathrm{s}} + P\,(x_{\mathrm{r}} + x_{\mathrm{op}}) = F_{\mathrm{s}} + \lambda_2\, w\, \frac{|x_{\mathrm{r}}| - x_{\mathrm{op}}}{x_{\mathrm{op}}}\, F_{\mathrm{s}}\ , \tag{8}$$

where $w$ is a weighting factor (of value of $30 \div 100$) and $\lambda_2$ is defined as:

$$\lambda_2 = \mathrm{sign}(x_{\mathrm{r}}) \quad \text{for} \quad |x_{\mathrm{r}}| \geq x_{\mathrm{op}}\ , \qquad \lambda_2 = 0 \quad \text{for} \quad |x_{\mathrm{r}}| < x_{\mathrm{L}}\ .$$

The spring force $F_{\mathrm{s}}$ is equal in general to the sum of linear and non-linear (due to the end-stops influence) components:

$$F_{\mathrm{s}} = F_{\mathrm{s,L}} + F_{\mathrm{s,NL}}\ . \tag{9}$$

In this case the operational range is approximately twice the linear range, hence $x_{\mathrm{op}} = 25\,\mathrm{mm}$ is assumed. The applied penalty weighting factor $w = 50$ was identified from the comparison of the time domain response signal measured during laboratory testing and numerical simulations. The value is approximate only and its variation by $\pm 20\,\%$ does not significantly change system behaviour.

The equation of motion of a damped system with both progressive end-stops ($k_{\mathrm{NL}}$) and stiff operational limits ($F_{\mathrm{s,PF}}$) for the case of $|x_{\mathrm{r}}| > x_{\mathrm{op}}$ is then:

$$m\,\ddot{x} + b\,\dot{x}_{\mathrm{r}} + k_{\mathrm{L}}\,x_{\mathrm{r}} + F_{\mathrm{s,NL}} + F_{\mathrm{s,PF}} + F_{\mathrm{f}} = 0\ , \tag{10}$$

where the friction damping force $F_{\mathrm{f}}$ has the form of:

$$F_{\mathrm{f}} = F_{\mathrm{fk}}\ \mathrm{sign}(\dot{x}_{\mathrm{r}}) = \mu_{\mathrm{k}}\,F_{\mathrm{N}}\ \mathrm{sign}(\dot{x}_{\mathrm{r}}) \tag{11}$$

and the relative displacement $x_{\mathrm{r}}$:

$$x_{\mathrm{r}} = x - u\ , \tag{12}$$

where $x = x(t)$ is the mass $m$ horizontal absolute displacement, $\ddot{x}$ its horizontal acceleration and $u = u(t)$ is horizontal displacement excitation.

The above-described formulation of an additional force to the equation of motion rapidly increases affinity of the numerical solution to instability. Therefore, in case of simulation, the time integration step-size $\Delta t$ has to be estimated carefully for the relative displacement region where the penalisation is applied.

### 2.4. End-stops parameter identification by the least squares method

Following the structural assumptions, the oscillatory system exhibits a range of displacements $(-x_{\mathrm{L}}, +x_{\mathrm{L}})$ within which a linear behaviour can be stipulated. The measured spring characteristic involves both the linear and non-linear components. For estimation of chosen parameter by regression analysis, both regions have to be treated separately, noting that the non-linear force response is a superposition of the response of the linear spring and the response of the end-stops.

| Measurement according to Fig. 2: | | course 1 | course 2 |
|---|---|---|---|
| Linear range | $x_{\mathrm{L}}$ [mm] | 10 | 10 |
| | $k_{\mathrm{L}}$ [$\mathrm{Nm}^{-1}$] | 9114 | 8512 |
| The exponential model | $A_2$ [N] | 15.672 | 20.906 |
| | $\beta$ [1] | 351.18 | 366.05 |
| | relative error [%] | 19.5 | 19.5 |
| The $\alpha$-root model | $A_3$ [$10^6\,\mathrm{Nm}^{-\alpha}$] | 4.156 | 7.500 |
| | $\alpha$ [1] | 1.912 | 1.966 |
| | relative error [%] | 9.5 | 17.4 |
| The cubic model | $k_{\mathrm{NL}}$ [$10^8\,\mathrm{Nm}^{-3}$] | 4.946 | 8.610 |
| | relative error [%] | 10.3 | 6.9 |
| The quadratic model | $k_{\mathrm{NL}}$ [$10^6\,\mathrm{Nm}^{-2}$] | 6.858 | 11.853 |
| | relative error [%] | 8.3 | 15.4 |

*Tab.1: Identified parameters for various models of the two suspension systems*

The measured system stiffness linear range was $x_{\mathrm{L}} = 10\,\mathrm{mm}$. As seen in Figure 2a, the course of the mean response force does not intersect the point of origin, $O = [0, 0]$. This might be caused either by measurement error or by assembly imperfection within mounting tolerances. For the purpose of least squares identification, this gap has to be removed by shifting the plot to the origin. The obtained results for all assumed regression models are listed in Table 1.

From Table 1 it is clearly seen that for the course 1 the quadratic approximation furnishes the best fit (the lowest relative error), while the course 2 is best approximated by the cubic course. The other two models furnish higher relative errors, hence the approximation is worst.

## 3. Apparent natural frequency of the system with end-stops

The end-stops implemented in the structure exhibit progressively growing force response and so they strongly influence the dynamical behaviour of the entire system. For example, the frequency of free-oscillation response on the initial relative displacement $x_0$ – system initial perturbation (keeping other initial conditions at zero) then depends on the interference of $x_0$ with the end-stops region [4]. For the initial displacement $|x_0| > x_{\mathrm{L}}$, such frequency is always higher than for the case of within the linear range $|x_0| < x_{\mathrm{L}}$ and increases with the further increase of $|x_0|$. Analytical investigation of the oscillatory system by the method of equivalent linearisation provides some insight into end-stops influence on the system natural frequency and sets a condition for estimation of system undesired behaviour under general form of input excitation.

The shift of the resonant frequency due to hits on structural limits was not analytically derived. The structural limits represent a hard restriction of the amplitude of relative displacement. The introduced substitutive mathematical description by the penalty force approach is only an idealisation of the nature of their influence. Moreover such an operational regime, during which the structural limits are under permanent impacting, is potentially detrimental both to the system and to the seated driver and should be avoided by all means. Under these assumptions, further analytical expansion of influence of their presence is not necessary at this stage.

Expressing the equivalent linear stiffness coefficient $k_{\mathrm{eq}}$ using the equivalence of potential energy was chosen as a proper method because of analogy with derivation of the equivalent damping coefficient in the system with friction damping. The estimation of the equivalent stiffness $k_{\mathrm{eq}}$ and thus the apparent natural frequency $\omega_{0\mathrm{A}}$ using the equivalency of the potential energy is less accurate than the commonly used harmonic linearisation method. However, especially in the case of restoring force given by a set of conditions different for $|x_0| < x_{\mathrm{L}}$ and $|x_0| > x_{\mathrm{L}}$ the method of equivalent potential energy is more straightforward and simpler to derive. For the purpose of further analysis it was considered to be sufficiently accurate, giving the lower bound estimation of $\omega_{0\mathrm{A}}$. As shown further, so obtained simulation results are in good agreement with experimental results.

Assuming that the total potential energy $E_{\mathrm{stot}} = E_{\mathrm{sL}} + E_{\mathrm{sNL}}$ is stored in both linear spring and in the progressive end-stops results for the relative displacement amplitude $\delta$ [8] into:

$$E_{\mathrm{stot}} = E_{\mathrm{sL}} + E_{\mathrm{sNL}} = \frac{1}{2}\, k_{\mathrm{L}}\, \delta^2 + E_{\mathrm{sNL}} \ , \tag{13}$$

For the general $\alpha$-root definition of the non-linear force $F_{\mathrm{s,NL}}$ the potential energy stored in the deformed end-stop unit is equal to:

$$E_{\mathrm{sNL}} = \frac{1}{\alpha + 1}\, k_{\mathrm{NL}}\, |\delta - x_{\mathrm{L}}|^{\alpha+1} \ . \tag{14}$$

Equivalent stiffness is then determined using the equivalent mechanical energy linearisation over the range $x_{\mathrm{r}} = \langle 0, \delta \rangle$.

$$\int_0^{\delta} k_{\mathrm{eq}}\, x_{\mathrm{r}}\, \mathrm{d}x_{\mathrm{r}} = E_{\mathrm{sL}} + E_{\mathrm{sNL}} \ . \tag{15}$$

Substituting formulas (13) and (14) for the linear and non-linear component of the potential energy into Eq. (15) for $\delta > x_{\mathrm{L}}$ follows:

$$\frac{1}{2}\, k_{\mathrm{eq}}\, \delta^2 = \frac{1}{2}\, k_{\mathrm{L}}\, \delta^2 + \frac{1}{\alpha + 1}\, k_{\mathrm{NL}}\, |\delta - x_{\mathrm{L}}|^{\alpha+1} \ . \tag{16}$$

Hence, for $\delta \leq x_{\mathrm{L}}$,

$$k_{\mathrm{eq}} = k_{\mathrm{L}} \tag{17}$$

and for $\delta > x_{\mathrm{L}}$,

$$k_{\mathrm{eq}} = k_{\mathrm{L}} + 2\, \frac{1}{\delta^2\, (\alpha + 1)}\, k_{\mathrm{NL}}\, |\delta - x_{\mathrm{L}}|^{\alpha+1} \ , \tag{18}$$

from which for the quadratic course of the end-stop force, described by Eq. (6), following formula results:

$$k_{\mathrm{eq}} = k_{\mathrm{L}} + \frac{2}{3}\, k_{\mathrm{NL}}\, \frac{(\delta - x_{\mathrm{L}})^3}{\delta^2} \ . \tag{19}$$

Introduction of an auxiliary relative variable $r_{\mathrm{x}} \geq 1$ defined by Eq. (20):

$$r_{\mathrm{x}} = \begin{cases} \dfrac{\delta}{x_{\mathrm{L}}} & \text{for} \quad |\delta| > x_{\mathrm{L}} \ , \\ 1 & \text{for} \quad |\delta| \leq x_{\mathrm{L}} \end{cases} \tag{20}$$

enables to simplify the formula of Eq. (19), assuming positive $x_{\mathrm{L}}$ only:

$$k_{\mathrm{eq}} = k_{\mathrm{L}} + \frac{2}{3}\, k_{\mathrm{NL}}\, x_{\mathrm{L}}\, \frac{(r_{\mathrm{x}} - 1)^3}{r_{\mathrm{x}}^2}\ . \tag{21}$$

This is the describing equation of the equivalent stiffness coefficient $k_{\mathrm{eq}}$, where $k_{\mathrm{eq}}$ is a function of the ratio $r_{\mathrm{x}}$ between magnitude of the relative displacement amplitude $\delta$ to the range $x_{\mathrm{L}}$ of linear stiffness. Note that for $\delta \leq x_{\mathrm{L}}$, $k_{\mathrm{eq}} = k_{\mathrm{L}}$ so for the whole operational range, the equivalent stiffness $k_{\mathrm{eq}} \geq k_{\mathrm{L}}$.

The estimation of the apparent natural angular frequency $\omega_{0\mathrm{A}}$ for the situation when the end-stops are engaged is derived using the standard formula $\omega_{0\mathrm{A}} = \sqrt{k_{\mathrm{eq}}/m}$, into which for $k_{\mathrm{eq}}$ is substituted from Eq. (21):

$$\omega_{0\mathrm{A}} = \sqrt{\frac{k_{\mathrm{L}} + \frac{2}{3}\, k_{\mathrm{NL}}\, x_{\mathrm{L}}\, \frac{(r_{\mathrm{s}} - 1)^3}{r_{\mathrm{x}}^2}}{m}} \tag{22}$$

Apparent natural frequency $\omega_{0\mathrm{A}}$ is a function of the ratio $r_{\mathrm{x}}$, and is always larger then undamped natural frequency $\omega_0 = \sqrt{k_{\mathrm{L}}/m}$ for the linear range, because $k_{\mathrm{eq}} \geq k_{\mathrm{L}}$.

Further assuming excitation by harmonic base displacement with angular frequency $\omega_{\mathrm{e}}$ equation of the skeleton curve is obtained by substituting $r_{\mathrm{x}}$ from Eq. (20) for $\delta > x_{\mathrm{L}}$ and expressing it from Eq. (22). For the quadratic function of the spring force the resulting formula is a cubic algebraic equation having three roots, two of them complex. Multiplying real root by $x_{\mathrm{L}}$ leads back to the relative displacement amplitude $\delta$. The plot of so calculated $\delta$ over the frequency range that covers linear system natural frequency $\Omega = \omega_{\mathrm{e}}/\omega_0$ creates a skeleton curve – the boarder-line between the under and above resonance regions (Figure 3).

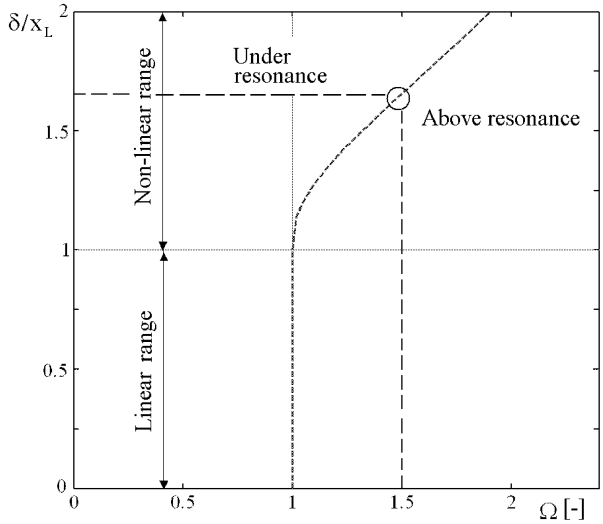


*Fig.3: Illustration of the course of apparent natural frequency due to the end-stops influence ($\Omega = \omega_{\mathrm{e}}/\omega_0$)*

The curves plotted in Figure 4 correspond to the amplitude-frequency characteristic of a described system under base kinematical harmonic excitation by effective acceleration

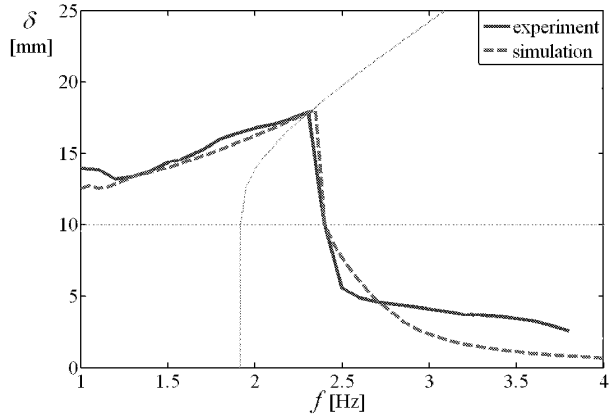


*Fig.4: Course of the relative displacement amplitude $\delta$ in the frequency domain*

value $a_{\mathrm{eff}} = 0.88\,\mathrm{m\,s^{-2}}$. Comparing the plotted courses a good match between the simulation and the experiment curves is seen.

## 4. Influence of initial displacement on the steady state response

The influence of the initial conditions (IC) on the output acceleration response of the non-linear system to the harmonic excitation is analysed next [5]. The initial relative displacement $x_0$ was chosen as the only non-zero initial condition (setting other to zero), as it can be easily visualised. It represents the initial potential energy present in the system at the beginning of the motion, which can influence the whole following trajectory. In the analysed system, certain level of the initial energy causes massive increase of the incidence of end-stops impacts. This can be shown in the plots of power spectral densities (PSD) as a presence of the region that significantly differs in shape and volume from that one, in which non-stationary action is either not dominant or not present at all.

The end-stops also shift system natural angular frequency from that one defined by the linear stiffness $\omega_0$ to the apparent one $\omega_{0\mathrm{A}}$ (given e.g. for the quadratic stiffness of the end-stops by the Eq. (22)).

### 4.1. Simulation of a system with zero damping

Simulations were performed using a harmonic signal $u(t)$ with the effective value of acceleration $a_{\mathrm{ueff}} = 0.70\,\mathrm{m\,s^{-2}}$, angular frequency $\omega_{\mathrm{e}} = 1.5\,\omega_0$ and a superimposed random noise component of 10 % with normal distribution of acceleration. Due to non-linear character of the system analysis has to be performed by averaging over a large number of realizations. The system is exposed to the same harmonic excitation, however each realisation might either start from randomly preset ICs within the linear range or due to the added small random component to the excitation signal has slightly different statistical properties [5].

The input acceleration signal parameters were chosen in such a way that the resulting linear steady state response relative displacement amplitude would be less than $x_{\mathrm{L}}$ so that in ideal case no end-stops would by involved. The excitation signal frequency was set to $\omega_{\mathrm{e}} = 1.5\,\omega_0$ so the transmissibility of the relative displacement $T_{\mathrm{xr}}$ of the linear undamped

system, defined by Eq. (23), at $\Omega = \omega_e/\omega_0 = 1.5$ is $T_{xr} = 1.8$.

$$T_{xr} = \left| \frac{\Omega^2}{1-\Omega^2} \right| . \tag{23}$$

The effective value $a_{ueff}$ of excitation acceleration was calculated implicitly for each realization from the given ratio $\delta/x_L$ by the formula:

$$a_{ueff} = \frac{1}{\sqrt{2}} \frac{\delta}{T_{xr}} \omega_e^2 . \tag{24}$$

The resulting amplitude $\delta$ of steady state oscillation for applied value of $a_{ueff}$ was well under $x_L$ ($\delta = 0.61\, x_L$). So if the unperturbed system reaches the steady state within the linear range resulting oscillations are assumed not been influenced by the end-stops. Contrary, if either the initial perturbation by $x_0$ or the displacement peak amplitude during the transient are sufficient to cause the end stops to be hit, system might retune and might start to oscillate near the apparent resonance frequency $\omega_{0A} = \omega_e$. The amplitude of oscillations which corresponds to response of the system in the state of apparent resonance of $\omega_{0A} = 1.5\,\omega_0$ would be equal to $\delta \approx 1.7\, x_L$, as can be derived from Eq. (22) and seen on Figure 3.

Results are illustrated in Figure 5. The acceleration transmissibility of the undamped linear system would be $T_a = 0.8$, while due to the non-linearities in the PSD plot appear peaks at $\omega_e$ higher harmonics. Therefore, for the stabilized steady state system oscillation, are within the linear range $(-x_L, +x_L)$ of relative displacement $x_r$. Ability of the system to extinct the transient state due to the IC perturbation is influenced by damping. Sufficiently perturbed IC might tend to retune the system, i.e. the amplitude of relative displacement that corresponds to the given $\omega_{0A} = \omega_e$ behaves as an attractor.

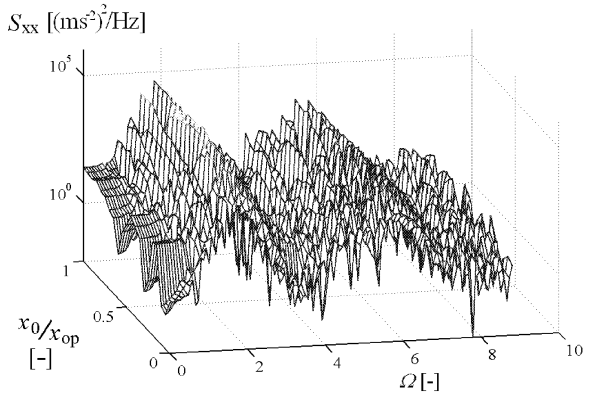


*Fig.5: PSD of the acceleration signal as a response to harmonic kinematical excitation at angular frequency* $1.5\,\omega_0$ *and for initial displacement* $x_0$*, damping* $\bar{\mu}_k = 0$*;* $\xi = 0$

Starting from the zero IC the relative displacement amplitude is expected to remain within the linear range. For a small or even zero damping once the end stops are involved into the course of oscillation an increased effective value (RMS) of the output acceleration will

result. Moreover, system might retune to the close neighbourhood of the point of apparent resonance frequency $\omega_{0\mathrm{A}}$. When the oscillations start, due to ICs, from the non-linear stiffness region and no sufficient damping is present the system permanently oscillates in this neighbourhood. The effective value of the output signal significantly increases comparing to the case when IC $\in \langle -x_{\mathrm{L}}, +x_{\mathrm{L}} \rangle$.

The influence of general damping (i.e. friction, hysteretic, viscous, etc.) to the reduction of non-stationary motion is simply analysed by plotting the course of coefficient of concurrence $\kappa$, Eq. (25), versus the damping ratio $\xi$ or the relative kinetic friction coefficient $\bar{\mu}_{\mathrm{k}}$. The coefficient of concurrence $\kappa$ is the ratio of acceleration RMS values obtained by averaging all $m$ realizations with the initial condition in non-linear range to the RMS value of all $n$ realizations with initial conditions within the linear range ($|x_0| < x_{\mathrm{L}}$), both obtained by the same averaging procedure, denoted by the acceleration RMS values averaging operator $E\{a_{\mathrm{x}}\}$ defined for the normal distribution function:

$$\kappa = \frac{E\{\mathrm{RMS}(a_{\mathrm{x,NL}})_{\mathrm{m}}\}}{E\{\mathrm{RMS}(a_{\mathrm{x,NL}})_{\mathrm{n}}\}} \,. \tag{25}$$

According to the Parseval's theorem [5], this quantification can be applied also on the course of the power spectral densities of the acceleration signal as a response on the identical excitation, however with varying initial displacement $x_0$ (within the operational range $x_{\mathrm{op}}$). Then the influence of the additional damping on the mitigation of the IC influence can be illustrated by series of surface plots (see Figure 6) with varying damping ratio $\xi$ or relative kinetic friction coefficient $\bar{\mu}_{\mathrm{k}}$.

i. For linear viscous damping the damping ratio $\xi$ is given in the standard way:

$$\xi = \frac{b}{2\sqrt{k_{\mathrm{L}}\, m}} \,. \tag{26}$$

ii. The dry-friction damping is described by a relative dimension-less kinetic friction coefficient $\bar{\mu}_{\mathrm{k}}$. For the assumed amplitude of excitation $F_0 = \sqrt{2}\, m\, a_{\mathrm{eff}}$ and for the friction force $F_{\mathrm{fk}}$ expressed using the friction coefficient $\mu_{\mathrm{k}}$ and the normal force $F_{\mathrm{N}} = m\, g$ (where $g$ is the gravity acceleration) [1], so that $F_{\mathrm{fk}} = \mu_{\mathrm{k}}\, m\, g$, the relative kinetic friction coefficient $\bar{\mu}_{\mathrm{k}}$ is defined in the following way:

$$\bar{\mu}_{\mathrm{k}} = \frac{4}{\pi}\,\frac{F_{\mathrm{fk}}}{F_0} = \frac{4}{\pi}\,\frac{\mu_{\mathrm{k}}\, g}{\sqrt{2}\, a_{\mathrm{ueff}}} \,. \tag{27}$$

### 4.2. Influence of single type of damping

The analysis was performed according to Eq. (25). Either the minimal viscous damping ratio $\xi$ or a minimal normalized friction coefficient $\bar{\mu}_{\mathrm{k}}$ were sought such as to extinct the non-stationary motion. For each level of harmonic excitation, the sets of output signals were obtained from the system initially perturbed within linear range and latter from within the non-linear range. Accelerations signals from these two groups of IC were compared. System was assumed to behave quasi-chaotically (i.e. the operation with irregular end-stops hits), if the coefficient of concurrence $\kappa$ was below the threshold value 1.1 and the steady state relative displacement stays within the linear range $(-x_{\mathrm{L}}, +x_{\mathrm{L}})$ at least for the initial displacement $x_0 = 0$. This secondary condition ($\delta < x_{\mathrm{L}}$ for $x_0 = 0$) is due to the fact that

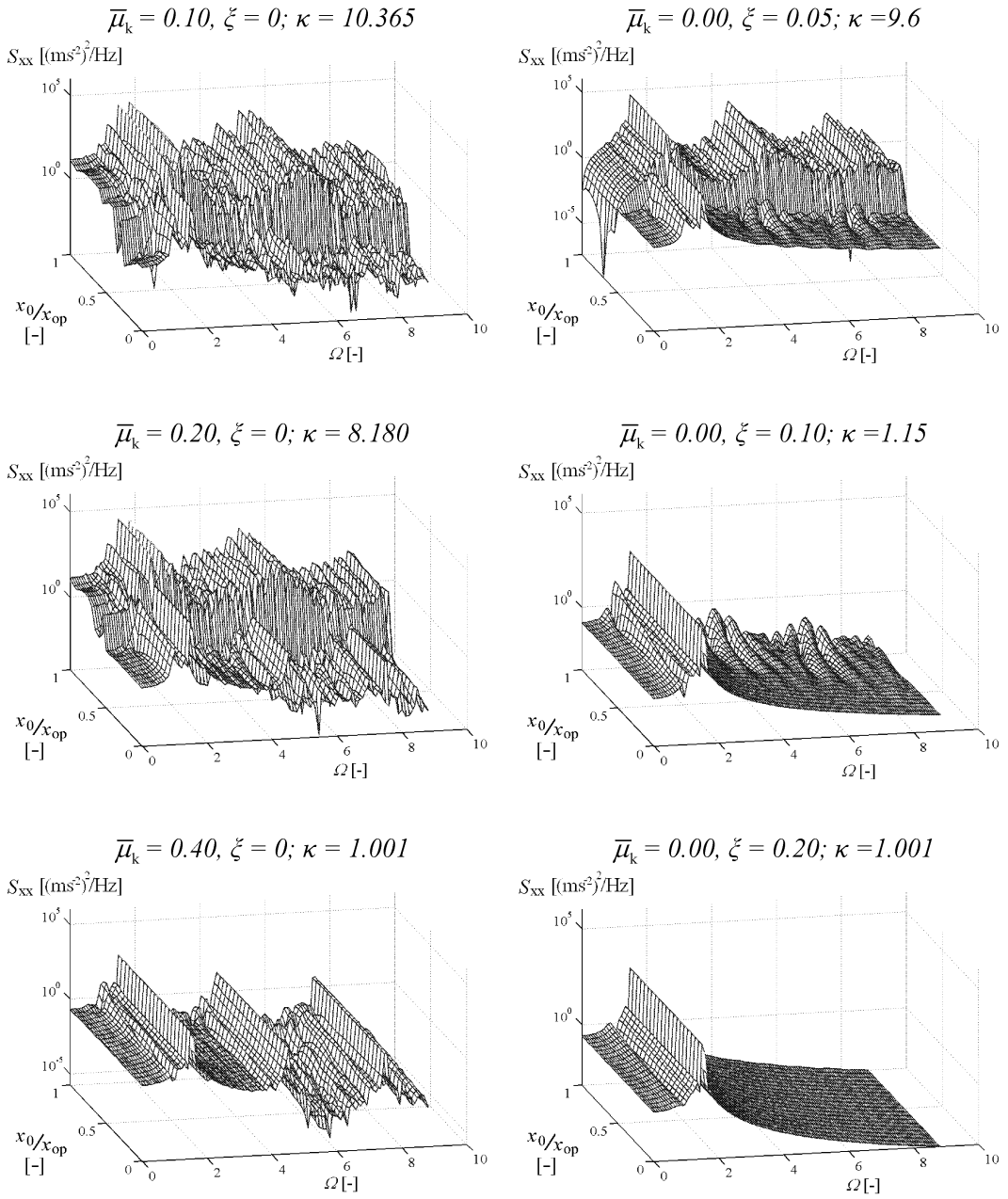


*Fig.6: PSD of the acceleration signal as a response to the harmonic kinematical excitation of the frequency of* $1.5\,\omega_0$ *and initial displacement* $x_0$

the concurrence coefficient $\kappa \to 1$ also in the case if the end-stop hit-to-hot oscillations are induced regardless of the value of initial displacement $x_0$ (see Figure 5). The chosen value of $\kappa \leq 1.1$ represents only an approximate threshold for numerical calculations. Following observation, the coefficient $\kappa$ either hovers around 1.0 (if the system behaviour is not influenced by varying IC) or $\kappa \gg 1$ for the damped system strongly influenced by the non-linear end-stops. The value of $\kappa \approx 1$ indicates that the transients due to the non-zero IC extinct

and the steady state system oscillations remain within the linear range. If $\kappa > 1.1$, system behaviour differs for $|x_0| > x_\mathrm{L}$ and for $|x_0| < x_\mathrm{L}$.

In Figure 6 in the left column the limit situation for variable $\bar{\mu}_\mathrm{k}$ and zero $\xi$ is depicted, representing a system with dry-friction only, whereas in the right column the situation with variable $\xi$ and zero $\bar{\mu}_\mathrm{k}$ is depicted, corresponding to viscous damping only. In these figures a sharp boundary between the non-stationary oscillations with high value of the acceleration PSD and the standard movement with lower acceleration PSD is sought.

From these graphs it can be concluded, that for the dry-friction damping a value of $\bar{\mu}_\mathrm{k} = 0.40$ suffices to fully damp the non-stationary oscillations, whereas for viscous damping the value $\xi = 0.20$ is sufficient. Note also the course of acceleration PSD (last row) – the oscillatory system with sufficient viscous damping exhibits the well-known course with large peak at the excitation frequency $\omega_\mathrm{e} = 1.5\,\omega_0$, whereas the oscillatory system with the sufficient dry-friction damping exhibits a number of odd harmonics of the excitation frequency $\omega_\mathrm{e}$.

### 4.3. Influence of combined damping

Obviously the courses illustrated in Figure 6 are limit cases. A case of the behaviour of the oscillatory system with the combined viscous and dry-friction damping is analysed next.

The combined damping is represented by a combination of values $\xi$ and $\bar{\mu}_\mathrm{k}$. The selected levels of excitation were given as a preset ratio of the steady state displacement amplitude $\delta$ to linear range limit $x_\mathrm{L}$ : $[0.5, 0.7, 0.9, 1.0, 1.1]$. Analysis was performed according to Eq. (25). Excitation signal frequency was set to $\omega_\mathrm{e} = 1.5\,\omega_0$; the RMS value of excitation acceleration was calculated implicitly for each realization from the given $\delta/x_\mathrm{L}$ by the formula Eq. (24).

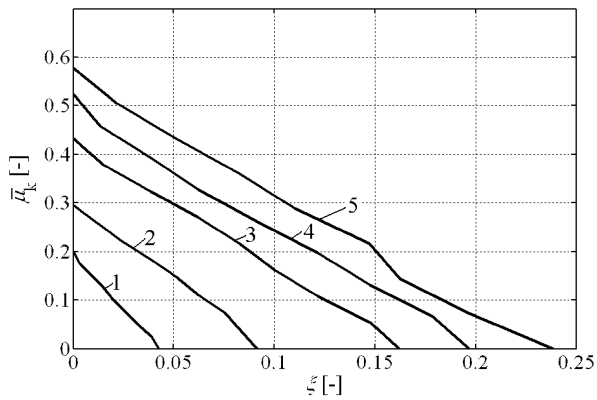


*Fig.7: Minimal values of damping ratio $\xi$ and friction coefficient $\bar{\mu}_\mathrm{k}$, 1 – $\delta/x_\mathrm{L} = 0.5$, 2 – $\delta/x_\mathrm{L} = 0.7$, 3 – $\delta/x_\mathrm{L} = 0.9$, 4 – $\delta/x_\mathrm{L} = 1.0$, 5 – $\delta/x_\mathrm{L} = 1.1$*

In Figure 7 the relations between $\bar{\mu}_\mathrm{k}$ and $\xi$ are plotted for each of the five above-mentioned excitations. It can be seen that the dependence is a straight line. The viscous damping is more effective than the dry-friction – the necessary characteristic variable $\xi$ limit value is approximately a half of the corresponding characteristic value $\bar{\mu}_\mathrm{k}$ for the dry-friction. Moreover, from this graph a value of the other characteristic variable can be estimated, if one of the characteristic variables ($\xi$ or $\bar{\mu}_\mathrm{k}$) is known beforehand and some level of relative displacement excitation can be assumed.

## 5. Conclusions

The search of the optimal model of the end-stops restoring force provided some models of the end-stops. In addition to the quadratic model treated in [8] further models were introduced, wherefrom the quadratic and cubic models proved as those approximating the measured courses best. These models are used in subsequent analysis of end-stops influence on the VIS performance. The engagement of the end-stop in the VIS induces a state of apparent resonance and partially influences the stability of such a system.

Viscous damping proved to be an effective tool to eliminate this inconvenient behaviour, as a damping ratio of approx. $\xi \cong 0.10-0.20$ provides sufficient stabilisation of the motion for the applied excitation acceleration signal. In contrast, the friction damping, due to its nature, does not exhibit this property and much higher relative kinetic friction coefficient values are needed to obtain the same effect. Surface plots in Figure 6 illustrate the sole influence of these values on oscillatory system behaviour. The graph in Figure 7 can be used to assess their mutual influence if a combined type of damping is assumed.

## Acknowledgement

This research was partially undertaken in conjunction with the Pan-European research project VIBSEAT (Contract No. GR3D-CT-2002-00827 of the European Commission) and within the Project No. 2/6161/26 of the Slovak VEGA Grant Agency for Science. Support of both Agencies is gratefully acknowledged.

## References

[1] Andreaus N., Casini P.: Dynamics of friction oscillators excited by a moving base and/or driving force, Journal of Sound and Vibration, 245, 2001, pp. 685–699
[2] Buchanan J., Turner P.: Numerical methods and analysis, McGraw-Hill, 1992, pp. 283–331
[3] Dumont Y., Paoli L.: Simulations of beam vibrations between stops: comparison of several numerical approaches, In Proceedings of ENOC 2005 Conference, TUV Eindhoven, Eindhoven 2005, pp. 1636–1643
[4] Fidlin A.: On the strongly nonlinear behavior of an oscillator in a clearance, In Proceedings of ENOC 2005 Conference, TUV Eindhoven, Eindhoven 2005, pp. 389–398
[5] Miláček S.: Náhodné a chaotické jevy v mechanice, Praha, Vyd. ČVUT, 2003
[6] Štecha J.: Optimální rozhodování a řízení, Praha, Vyd. ČVUT, 2002, pp. 121–134
[7] Zahoranský R., Stein J., Chmúrny R.: Dry-friction effects modelling in kinematically excited vibration isolation systems, In Proceedings of the Dynamics of Machines 2005 Colloquium, IT CAS, Prague 2005, pp. 155–162
[8] Zahoranský R., Stein J., Meyer H.: Modelling and simulation of kinematically excited vibration isolation systems with friction under random and harmonic excitation, In Proceedings of ENOC 2005 Conference, TUV Eindhoven, Eindhoven 2005, pp. 2663–2671
[9] Zahoranský R., Stein J.: Modelling and evaluation of the influence of end-stop impacts on response signal in a vibration isolating system, In Proceedings of the Dynamics of Machines 2006 Colloquium, IT CAS, Prague 2006, pp. 175–182

*Received in editor's office*: March 16, 2006
*Approved for publishing*: October 10, 2006

*Note*: The paper is an extended version of the contribution presented at the national colloquium with international participation *Dynamics of Machines 2006, IT AS CR, Prague, 2006.*